# Measurement and Analysis of Brake and Tyre Particle Emissions from Automotive Series Components for High-Load Driving Tests on a Wheel and Suspension Test Bed

Martin Kupper *, Ludwig Schubert, Manfred Nachtnebel, Hartmuth Schröttner, Michael Peter Huber, Peter Fischer, Alexande Bergmann

Posted Date: 19 February 2024

doi: 10.20944/preprints202402.1000.v1

Keywords: Non-Exhaust Emissions; Brake Wear Aerosol; Particle Measurement; Ultrafine Particles; Electron Microscopy

 doi:10.20944/preprints202402.1000.v1



*Article*

# Measurement and Analysis of Brake and Tyre Particle Emissions from Automotive Series Components for High-Load Driving Tests on a Wheel and Suspension Test Bed

**Martin Kupper [1,*], Ludwig Schubert [2], Manfred Nachtnebel [3], Hartmut Schröttner [3,4], Michael Peter Huber [2], Peter Fischer [2] and Alexander Bergmann [1]**

1 Institute of Electrical Measurement and Sensor Systems, Graz University of Technology, 8010 Graz, Austria
2 Institute of Automotive Engineering, Graz University of Technology, 8010 Graz, Austria
3 Austrian Centre for Electron Microscopy, 8010 Graz, Austria
4 Institute of Electron Microscopy and Nanoanalysis, Graz University of Technology, 8010 Graz, Austria
* Correspondence: martin.kupper@tugraz.at; Tel.: +43 316 873 30585 (M.K.)

**Abstract:** The up-to-date challenge towards clean road transport are non-exhaust emissions. Important advances regarding measurement systems, including well defined characterisation techniques, as well as regulation, will happen in the next few years. In this work we present detailed results of particle emissions from a test bed for wheel suspension and brakes, consisting of aerosol (size distribution, particle number (PN) and mass (PM)) and electron microscopy measurements (EM) under different load conditions. Standard tyres and brakes from series production were tested with a high-load driving cycle while particle measurements were conducted by gravimetric measurements and with a TSI SMPS, a TSI APS and a GRIMM OPS. Furthermore, samples were analyzed by electron microscopy. A bimodal particle size distribution (PSD) was obtained with the SMPS, with peaks at 20 nm and around 400 nm. EM analysis of >1400 single particles from the electrostatic sampler matches the PSD results. EM analysis also showed ultrafine particles, mainly from O, Fe, Si, Ba, Mg and S and also fractal particles with high C fractions. Our results suggest, in agreement with previously published literature, that particulate emissions are related to brake disc temperature and occur in significant amounts above a threshold temperature.

**Keywords:** non-exhaust emissions; brake wear aerosol; particle measurement; ultrafine particles; electron microscopy

## 1. Introduction

In the last decades, efforts to limit air pollution were successful. In Europe the concentrations of pollutants in the air are constantly decreasing, but air pollution in urban areas is still a major health concern [1]. The vast majority of Europeans living in cities are exposed to particulate matter (PM) levels above the WHO limit [2]. As particulate exhaust emissions from transportation, the largest emitter in recent decades, are nowadays heavily regulated, other sources come to the fore. Brake Wear (BW) and Tyre Wear (TW) particulate emissions, together with road surface wear comprised as non-exhaust particle (NEP) emissions. NEP have been studied for decades, as they contribute at least half to the ambient PM which can be accounted to transport [3] and can reach up to 90 % [4]. The contribution of BW to NEP is ranging from ∼16 % to >50 % [3,5,6] and the contribution of TW to NEP from ∼5 % to >30 % [6,7]. An almost equal contribution of NEP and exhaust emission to total traffic related PM10 was already known 10 years ago [5] and the ever-increasing and eventually overwhelming proportion of electrified vehicles (EV) will continuously increase this fraction, as the emission of NEP is of relevance also for EVs [8–10]. As a consequence to these trends, first regulation efforts led to an harmonised procedure for the laboratory measurement of brake emissions for light-duty vehicles, specified in the Global Technical Regulation (GTR) 24 of the UNECE. The latest European emission

 doi:10.20944/preprints202402.1000.v1



legislation EURO 7 relates to the GTR 24 and furthermore introduces emission limits for BW and abrasion limits for TW, as it was e.g. announced by a press release of the European Commission in December 2023 [11].

Current research on NEP covers measurement techniques, the characterisation of emissions and fundamental formation mechanisms. The Euro 7 legislation compliant method for brake wear (BW) particles is one centre of research. A global interlaboratoy study was coordinated by the Particle Measurement Programme (PMP) informal working group of the UNECE [12,13], to assess and compare possible established measurement setups [14]. This ultimately lead to the definition of UN GTR 24, which was adopted for Euro 7. The emissions of a single brake have to be measured on a fully encapsulated brake test bed following the newly defined "WLTP-Brake" cycle. The harmonised methodology ensures representative and precise measurement of particle mass and particle number (PN). In this context the measurement of Total Particle Number (TPN), additionally to th for engine emissions established Solid Particle Number (SPN), was considered as relevant [15]. Comprehensive studies on NEP measurement and sensor techniques identified two main principles for NEP measurement [16]. According to UN GTR 24, PM10 and PM2.5 emissions shall be determined by gravimetric filter weighting, with two separate filter holders and cyclones for each cut-off diameter. PN shall be measured in terms of TPN10 and SPN10 with a nominal particle size of approximately 10 nm electrical mobility diameter and larger. This involves PN pre-classifiers, such as a 2.5 µm cyclone to remove larger particles, a dilution system with one or more dilution stages, an optical Particle Number Counter (PNC), and a volatile particle remover if SPN is measured.

Efforts are also tackling new sampling technologies for Real Driving Emissions (RDE) of BW particles, to quantify the on-road emissions in traffic and challenge the defined test bed procedure of the GTR 24 for it's representativeness. Brake temperatures, i.e. the brake disc temperature (BDT), are recognised impacting PM and PN brake emissions [3,10], especially after exceeding a critical threshold temperature, potentially releasing volatile particles with a mode at 10 nm to 30 nm [14,17]. Defined cooling conditions on the test bed keep the brake temperature well below this threshold. In reality, the temperature behaviour of a brake system is directly impacted by various factors, including ambient conditions, changes in elevation, driving habits, vehicle design, and recuperation strategy. Therefore, assessing the inherent cooling characteristics of a particular vehicle's brakes plays a pivotal role in evaluating its actual BW emissions [18,19].

The progress with tyre wear (TW) is not as far advanced as for BW, although it is the source of ∼5 % of total ambient PM. While this is only a small fraction (2 % to 5 %) which becomes airborne, the majority of TW is contributing to the global microplastics contamination [7,20]. For this reason, the UNECE founded the Task Force on Tyre Abrasion (TFTA) in 2022 to elaborate a future standardised test procedure for the reproducible measurement of TW. The vehicle convoy method on public roads, and the indoor drum dynamometer method are currently evaluated. However, the current objective is limited to a method for measuring TW by weight loss in order to quickly achieve a reduction in microplastics on European roads. Whether a method for determining airborne tyre emission particles will also be developed in the future remains to be seen and is currently only the subject of research projects [7,21–23].

Measurement of NEP is also a challenge on the sensor level, as NEP aerosols are of very heterogeneous composition and cover a broad size range, as it is shown by the results of this work in accordance to literature [3,20]. This is in contrast to the since decades in the automotive environment established exhaust particle measurement, where always soot particles are measured [24,25]. The PNC which is typically used for the SPN and TPN measurements are Condensation Particle Counters (CPC) [9,13,18], which are known to show material dependency [26–28]. Electrical spectrometers, which are often used for the size distribution measurement, depend on the effective particle density, which is generally unknown, different for particles of different material, also strongly affected by the brake pad formulation and particle size [16]. The topic of sensors for reliable NEP detection should be considered for future research efforts.

 doi:10.20944/preprints202402.1000.v1



In this work we present results from NEP aerosol measurements and EM analysis, done at a wheel and suspension test bed with a closed ventilation system. A fully automated 200 s high-load drive cycle was repeated in total 1100 times in sets of 20 consecutive repetitions. We characterised the NEP regarding size distribution and number concentration with aerosol instrumentation at varius sampling positions and with EM for size distribution and chemical composition from a filter sample and dedicated samples from an electrostatic sampler. The total wear was assessed by gravimetric methods.

## 2. Materials and Methods

All measurements have been carried out at the wheel and suspension test bed, which is described in detail below. It is a component test bench for any complete wheel carrier, including the complete brake system, rim and tyre. It is equipped with a closed ventilation system, by which it is possible to measure the total particle emissions from the components in the test bed. Particle measurements have been done with aerosol instrumentation and by electron microscopy (EM) analysis of filters and dedicated samples.

### *2.1. Wheel and Suspension Test Bed*

The test setup, as illustrated in Figure 1(a), entails a steerable steel drum designed to apply a specific skew angle. The drum is coated with an abrasion-resistant layer, which is based on a real road surface with similar friction values. Moreover, the test bed is equipped with both a master cylinder, regulating brake pressure, and a hydraulic cylinder, controlling vertical forces. Two motors, one inside of the drum and another dedicated to wheel propulsion, have the capability to regulate drive torque and induce a specific slip on the tyre.

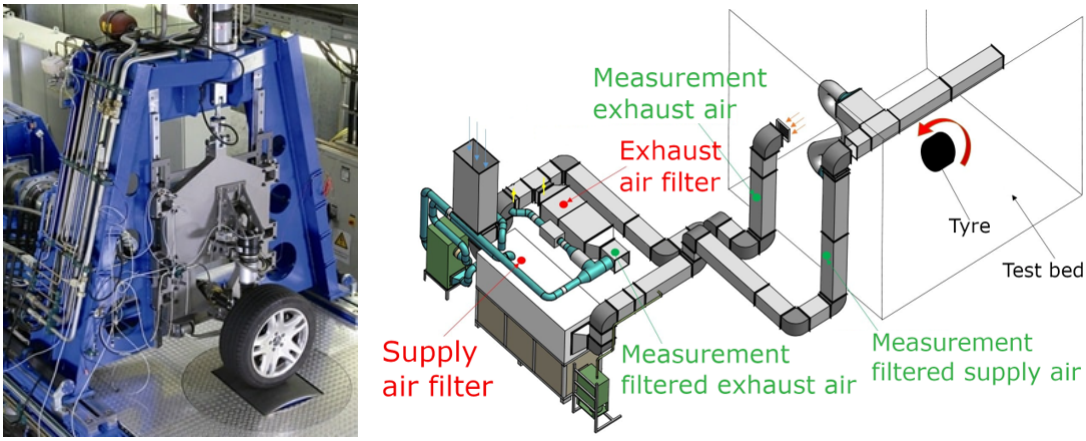


(a) CAD rendering of the test bed.

(b) Schematics of the ventilation with the sampling positions indicated in green and the filter positions in red.

**Figure 1.** Visualisation of the wheel and suspension test bed at the Institute of Automotive Engineering at the Graz University of Technology.

For the test program described below, a front axle chassis of a passenger car was mounted on the test bed. The entire car had a weight of 2781.5 kg. The tyres used were Continental ContiSportContact 5 summer tyre, with specifications 255/45 R22 107 XL. The composition of the brake pads was unknown, whereas the brake discs utilized were of gray iron construction.

A special characteristic of the test bed is the closed ventilation system, shown in Figure 1(b). Intake air with a volume flow of 2707 $m^3\,h^{-1}$ from the environment is led in a continuous flow through the supply air filter and passed into the measuring room via several ventilation outlets. The exhaust air is displaced through one ventilation opening and led through the exhaust air filter, before ventilated into the environment. The filters are described in the "Aerosol Measurement" section.

Preprints.org (www.preprints.org) | NOT PEER-REVIEWED | Posted: 19 February 2024 doi:10.20944/preprints202402.1000.v1



### 2.2. Test Program

The basis of the test program was a well-defined high-load cycle of 200 s, which was repeated fully automated consecutively in sets of 20 repetitions. Each set was followed by a pause to cool off the components, change the measurement position of the aerosol instrumentation and, if necessary, service and control work. At a single test day 5 sets were driven, the brake pads and tyres were exchanged for unused ones after each day. Brake pads and tyres were weighted before and after use. The tests were done at 11 sequential days, thus in total 1100 repetitions of the 200 s cycle have been done. For the supply air and the exhaust air of the ventilation system of the test bed dedicated, new air filters have been installed for the execution of the test program, which have also been weighted before and after installation. The filters are described in the "Aerosol Measurement" section.

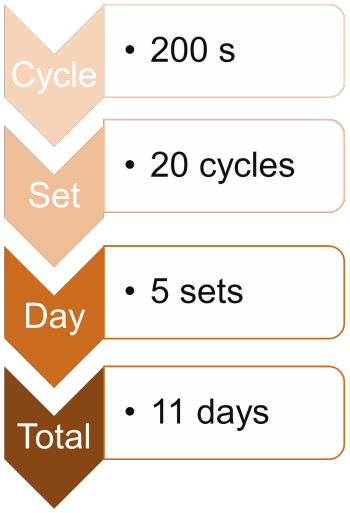


(a) Schematic of the timetable.

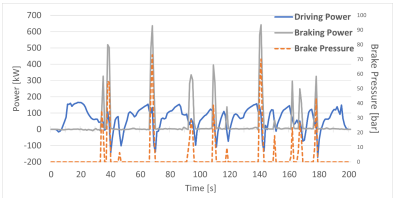


(b) Brake power and pressure.

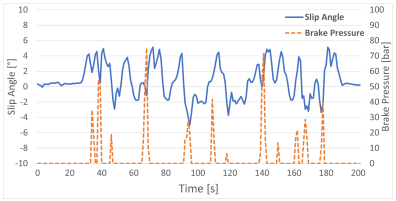


(d) Slip angle

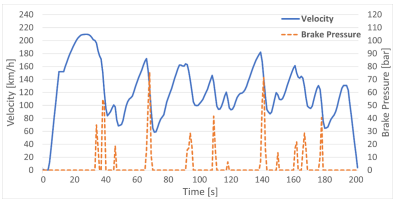


(c) Velocity

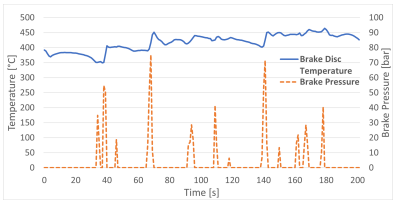


(e) Brake disc temperature

**Figure 2.** Representation of the used test program at the wheel and suspension test bed.

The test cycle was fully defined by time dependent set values regarding roller drive speed, drive torque, driving force, braking pressure, wheel vertical force, wheel vertical position, lateral force, suspension strut travel, pivot angle of the roller and air stream. A table with representative test cycle parameters is available in the supplementary online.

During each cycle the following parameters have been measured and recorded by the test bed operating system: Time, suspension strut travel, slip angle, wheel vertical force, roller drive speed, driving force, pressure at the brake cylinder, flywheel torque, ambient temperature, wheel vertical position, drive torque, braking torque, lateral force, BDT, tyre tread temperature (at left, mid and right) and driven distance.

### 2.3. Aerosol Measurements

We measured the PN concentration and the Particle Size Distribution (PSD) of ultrafine and larger particles, determined the airborne PM by gravimetric methods and collected samples of particles for electron microscopy analysis. Aerosol measurements have been carried out at the three measurement positions, indicated in Figure 1(b) in green with all instruments. Measurements have been also done inside the test bed with the APS described below and a custom made electrostatic sampling device for electron microscopy analysis.

For the aerosol measurements a TSI 3775 Condensation Particle Counter (CPC) was used for the measurement of PN concentrations of ultrafine particles (UFP). According to the manufacturer specifications, the TSI 3775 detects particles fully down to a diameter of roughly 10 nm, then with a detection efficiency of 50 % at 4 nm and 10 % at roughly 1.5 nm. In combination with a TSI 3081 Differential Mobility Analyser (DMA) and a TSI 3080 electrostatic classifier, equipped with a TSI

 doi:10.20944/preprints202402.1000.v1



3077 X-Ray source, an Scanning Mobility Particle Sizer (SMPS) setup is formed to measure the PSD of UFP. For larger particles a TSI 3321 Aerodynamic Particle Sizer (APS) was used, which allows to measure the PN concentration and PSD for aerosol particles in the size regime from 0.37 µm to 20 µm. Additionally a Grimm Dustdecoder 11-D (Optical Particle Spectrometer - OPS), which measures the PN concentration and PSD for aerosol particles in the size regime from 0.253 µm to 35.15 µm, was available, but its usage was limited due to an occurred malfunction. By knowledge of the PSD, the PM concentration can be estimated by assumption of a mean particle density.

Samples for the electron microscopy analysis have been collected by a custom made electrostatic sampler, with four deposition stages operated at different voltages to separate for different mobility diameters, details can be found in Appendix A. The set voltages were 200 V, 400 V and 800 V, as well as one with 0 V potential for reference. For singly charged particles this would mean a deposition of particles up to mobility diameter 62 nm for 200 V, 91 nm for 400 V and 136 nm for 800 V. See B for the theoretical details.

As described above, new filters for fresh and exhaust air in the test bed ventilation system have been installed before the testing and have been used for gravimetric analysis of the airborne PM. The used filteres were Kappa Wavebionix® with a filtration efficiency of 97.2 % at 28 nm, according to the manufacturer data sheet.

### *2.4. Electron Microscopy Analysis*

For EM analysis two kinds of samples were available. First the exhaust air filter was analysed and second particles were sampled by an electrostatic sampler inside the test bed. The dimensions of the electrostatic deposition plates in the sampler match the possible sample sizes of the EM devices and have been analysed directly. For the exhaust air filter, EM samples had to be prepared according to the method described in [29]. The filter was cut open and particles removed by shaking of the filter, with the opening pointing downwards above a prior cleaned container. A small, representative part of gained material was carefully filled into a glass, and positioned below carbon tape stripes, with the adhesive side pointing down. The particle material was swirled by a CO2 blast from the vessel, causing an assumed representative distribution of particles on the adhesive carbon tape. The tape stripes were then used as samples in the EM analysis.

All samples have been investigated using automated particle analysis by the combination of Scanning EM (SEM) and Energy Dispersive X-Ray Spectroscopy (EDX). Therefore, a Zeiss Sigma 300 VP equipped with an Oxford X-max N80 EDX detector was applied. For the automated acquisition and analysis of the particles, the Oxford built-in Aztec 3.4 software was used. Appropriate image thresholding of acquired Back-Scattered Electron (BSE) images was used for the segmentation between background (substrate) and particles. Image stacking was performed to analyse sufficient big areas obtaining the particle counts stated in the next chapter. For the stated particle sizes in the PSD the Equivalent Circular Diameter (ECD) was chosen, which was calculated from the measured projected particle areas.

## 3. Results

### *3.1. Gravimetric Measurements*

To assess the total wear mass, the used brake discs, brake pads and tyres were weighted before installation in the test bed and again after removal. The results can be seen in Table 1. In total 1345 g of mass was removed during the test drives, of which 70 % coming from the tyres.

The air filters from the ventilation system have been also weighted before and after installation. For the fresh air filter a small weight change of 12 g could be determined, the exhaust air filter gained 338 g of mass. Thus 25.13 % of the total wear mass was found in the exhaust air filter.

 doi:10.20944/preprints202402.1000.v1



**Table 1.** Measured weight differences.

| Component | Weight difference |
|---|---|
| Brake Discs Total | −71 g |
| Brake Pads Total | −306 g |
| Tyres Total | −968 g |
| Total Wear | −1345 g |
| Fresh Air Filter | 12 g |
| Exhaust Air Filter | 338 g |

### *3.2. Size Distribution Measurements*

The measured data from SPMS and APS were combined to show the PSD over the total covered range. The device combination was used at sampling positions for filtered supply air, exhaust air and filtered exhaust air in the ventilation system of the test bed, as indicated in green in Figure 1(b). The APS and the Grimm device have been also used for measurements inside the measurement room of the test bed. The results can be seen in Figure 3. It was not possible to acquire reliable PSD data with the Grimm device due to malfunction.

As described above, PM values can be derived from the PSD, by assumption of a mean particle density. As the mean density of the measured particles is not known, a calculation with the density of soot helps to contextualise the detected amounts. The estimated PM values were between 300 µg m$^{-3}$ to 400 µg m$^{-3}$ with maximum values at 450 µg m$^{-3}$.

As described above, by EM analysis of the exhaust air filter it was possible to determine a PSD, which can be seen in superposition to the exhaust air measurements done with the SMPS and the APS in Figure 3(c).

In the filtered supply air the PSD has only been measured by the SMPS due to the small sizes, as it can be sen in(Figure 3(a). The thus induced particle background, which is an order of magnitude below the measured values in the exhaust air flow, was not taken into account for further evaluation.

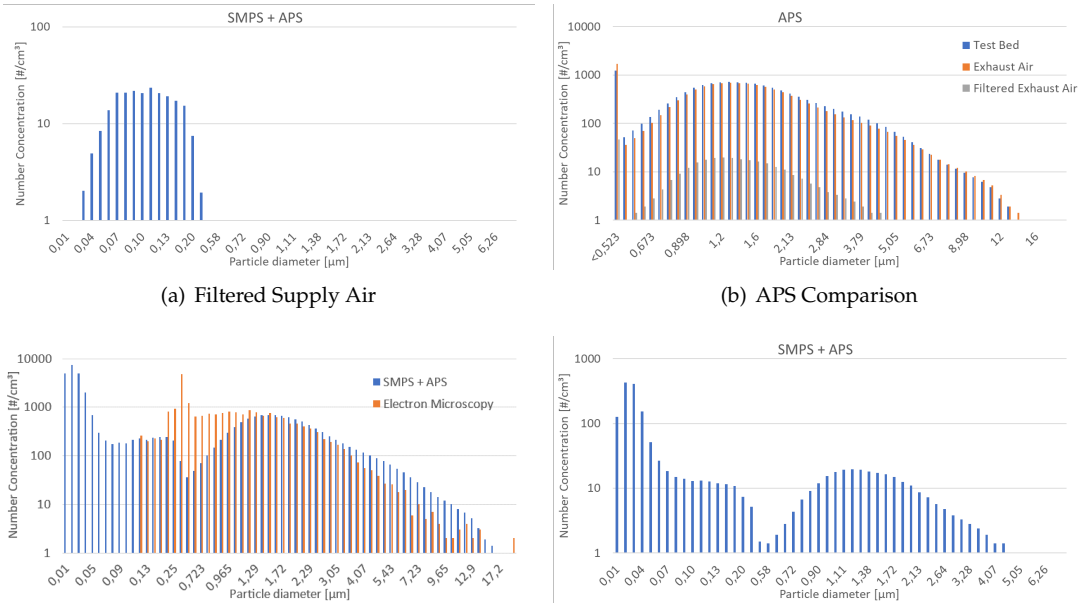


(a) Filtered Supply Air

(b) APS Comparison

(c) Exhaust Air

(d) Filtered Exhaust

**Figure 3.** Plots of the PSD data for different sampling positions and measurements. The scale of the x-axis was adopted for every plot to the visible data.

 doi:10.20944/preprints202402.1000.v1



### 3.3. Particle Number Concentration Measurements

From the raw data from single cycles, as exemplary shown in Figure 4(a), it can be recognised, that the PN concentration becomes comparable in between the cycles from the third cycle on. Analysis of the BDT measurements showed that the BDT also levels off from the third cycle on. Thus, we did not consider the first two cycles of each set for further analysis.

The PN concentration changes in relation with brake events and a change in BDT, as it can be seen in Figure 4(b). A linear scale was chosen for the PN concentration in this visualisation to make the changes better visible. Each brake event is followed by an increase in temperature, with the extend depending on the brake pressure. For the strong brake events the increase in temperature is then followed by an increase in the UFP PN concentration.

Comparing the data from the filtered and unfiltered exhaust air shows that the exhaust air filter reduces the UFP concentration one order of magnitude, thus roughly 90 % of the UFP PN concentration is captured in the filter.

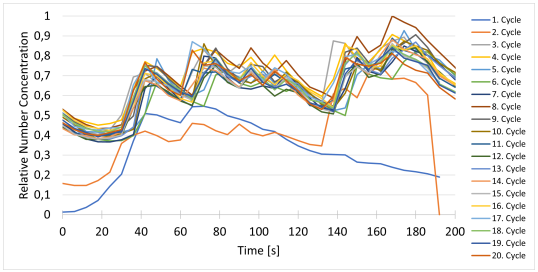


(a) Raw relative PN concentration data over one set (20 cycles).

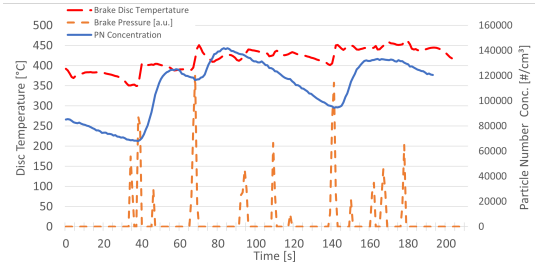


(b) Mean CPC PN concentration data of one set measured in exhaust air in linear scale.

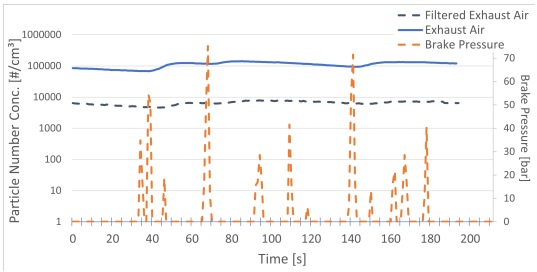


(c) CPC PN concentration data in logarithmic scale for comparison of unfiltered and filtered exhaust air.

**Figure 4.** Plots of the PN data for different sampling positions and measurements.

### 3.4. Electron Microscopy Measurements

All samples have been scanned automated and identified single particles have been analysed for size and composition. For the samples created from the exhaust air filter, the PSD can be seen in Figure 3(c) together with the corresponding PSD acquired with aerosol instrumentation. The PSD from the different depositions stages of the electrostatic sampler can be seen in Figure 5(a) and the corresponding total numbers are listed in Table 2. The found particle sized do not match the expected sized according to the calculations. The found separation of particles between the deposition stages was rather by structural properties, exemplary EM images of the three deposition stages can be seen in Figure 5, the 0 V reference plate was found to be particle free.

 doi:10.20944/preprints202402.1000.v1



**Table 2.** Number of particles determined by EM single particle analysis.

| Location | Number of particles |
|---|---|
| 0 V deposition voltage | 0 |
| 200 V deposition voltage | 7371 |
| 400 V deposition voltage | 6374 |
| 800 V deposition voltage | 2758 |
| Total | 16 503 |

Analysis of the particles composition was done by EDX, the results can be seen in Table 3. As the plates in the electrostatic sampler were made from copper and the sample tape for the samples from the filter were mainly made from carbon, the results for these elements have to be neglected for these samples. Since the particles are very small compared to the electron beam, an EDX-signal from the substrate is also generated in any measurement. Due to this circumstance and further conditions, like inhomogeneity and structure of the particles, the results have to be seen as semi-quantitative analysis. Nevertheless, as thousands of particles are measured, the analysis gives a valid insight into the mean composition of the particles. If particles were identified with a composition of pure substrate, they have been automatically omitted.

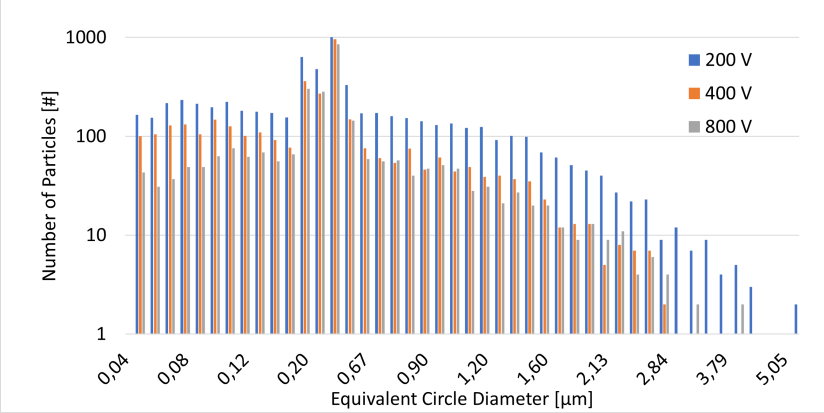


(a) PSD distribution determined by EM single particle analysis.

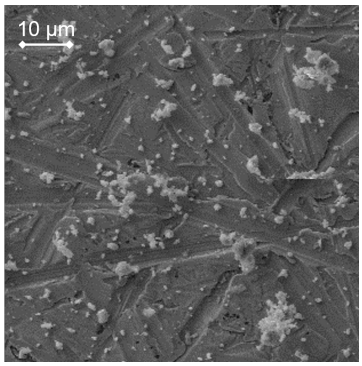


(b) Particles sampled with 200 V.

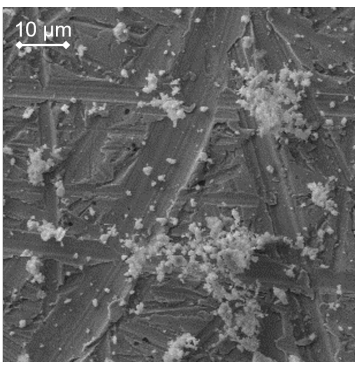


(c) Particles sampled with 400 V.

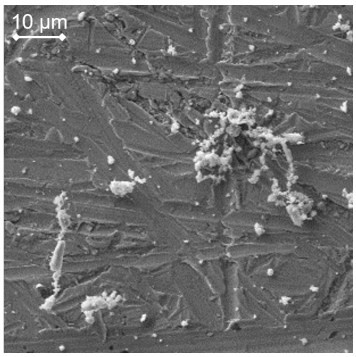


(d) Particles sampled with 800 V.

**Figure 5.** Results from the EM analysis. a) shows the obtained ECD from the single particle analysis of the deposition plates. b), c) and d) show exemplary regions of the deposition plates for the different voltages to illustrate the differences of the particles found.

 doi:10.20944/preprints202402.1000.v1



**Table 3.** Results of the composition analysis. The substrate material Cu for the electrostatic sampler and C for the filter is indicated in grey. The first column gives the fraction of particles found, containing the concerned element. The second column gives the mass fraction of the concerned element in relation to the total analysed mass.

| | 200 V | | 400 V | | 800 V | | Filter | |
|---|---|---|---|---|---|---|---|---|
| Element | # / % | wt / % | # / % | wt / % | # / % | wt / % | # / % | wt / % |
| Cu | 98,05 | 36,4 | 100,00 | 33,1 | 99,61 | 66,9 | 0,10 | 1,6 |
| O | 94,99 | 9,2 | 89,28 | 7,5 | 83,73 | 8,7 | 95,70 | 16,9 |
| Fe | 88,30 | 10,2 | 85,59 | 8,8 | 51,57 | 10,6 | 38,40 | 10,4 |
| Si | 59,64 | 3,2 | 70,52 | 2,7 | 41,18 | 3,1 | 99,80 | 1,0 |
| Ba | 62,12 | 4,3 | 60,30 | 2,8 | 33,53 | 3,8 | 24,20 | 2,9 |
| Si | 57,94 | 1,3 | 50,59 | 0,9 | 25,49 | 1,3 | 25,80 | 1,9 |
| Mg | 50,70 | 2,0 | 61,47 | 2,2 | 9,41 | 0,9 | 12,80 | 1,4 |
| C | 39,00 | 19,3 | 9,88 | 18,1 | 96,47 | 17,2 | 100,00 | 70,0 |
| Zr | 20,61 | 1,6 | 14,24 | 1,8 | 6,86 | 2,3 | 3,00 | 1,0 |
| Ca | 11,98 | 0,8 | 13,07 | 0,5 | 4,12 | 0,6 | 7,00 | 0,3 |
| Zn | 9,75 | 3,8 | 6,20 | 3,0 | 4,31 | 4,2 | 7,90 | 1,8 |
| Al | 3,90 | 2,3 | 6,53 | 2,4 | 0,59 | 0,7 | 0,60 | 0,5 |
| K | 2,51 | 0,6 | 0,84 | 0,4 | 1,18 | 1,7 | 0,40 | 0,5 |
| Cl | 1,39 | 0,6 | 1,34 | 0,3 | 4,51 | 0,6 | 0,04 | 0,3 |
| Cr | 0,56 | 1,2 | 3,18 | 1,6 | 0,20 | 1,0 | 0,30 | 0,9 |
| Br | 0,56 | 0,7 | 1,01 | 1,6 | - | - | - | - |
| P | 0,28 | 1,8 | 0,34 | 1,6 | 0,39 | 3,2 | 9,68 | 0,9 |
| Sn | 0,28 | 2,1 | 2,18 | 0,9 | - | - | 0,30 | 1,6 |
| Sr | 0,28 | 1,3 | - | - | - | - | - | - |
| Ti | - | - | 2,01 | 1,5 | 0,59 | 3,1 | 0,30 | 1,1 |
| Pb | - | - | - | - | 0,20 | 3,4 | - | - |

## 4. Discussion

From the gravimetric results in Table 1 it can be seen that a considerable amount of wear mass was produced, of wich about 25 % of it was found in the exhaust air filter. The observation, that at least a quarter of the total mass loss of the components was found to be airborne, must be seen differentiated. A possible generalisation is not indicated, as the chosen drive cycle was targeting maximised wear of the components in a minimum of time, to optimise the use of the operation time of the test bed. Driving the cycle with a vehicle is not possible. Furthermore, the reached BDTs of around 400 °C are possible, but not frequently expected for passenger car use and are also not considered in the WLTP-brake cycle [18,19,30], although the critical temperatures for ultrafine particle emission is considered below or around 200 °C [6,31].

Regarding the distribution of the lost mass of the components in relation to the total mass found in the filter, the results match latest literature. According to [7] about 2 % to 5 % of TW is airborne. For the measurements presented here, 2 % to 5 % correspond to 19.36 g to 48.8 g. If this estimated airborne fraction of the TW is summed up with the 306 g of the mass lost at the brake discs, this adds up to about the 338 g found in the exhaust air filter.

It is not possible to make any conclusions about PM not captured in the filter, as the ventilation system of the test bed is not optimised for aerosol transport and has unknown particle losses. Also the filtration efficiency of the exhaust air filter given by the supplier unfortunately does not allow any conclusions.

The obtained PSD is consistent over different methods and sample positions. Most impressive is the good match of the combined SMPS and APS data with the EM data in Figure 3(c), where also shape of the PSD and absolute numbers coincide mostly. The PSD shows a bimodal distribution with one distinct peak in the UFP region around 20 nm and around 400 nm. Most likely the bimodal shape is not representing the real distribution. The aberration between 250 nm to 723 nm is very likely due to the transition region between the instruments, where the SMPS shows deviations at it's upper size

 doi:10.20944/preprints202402.1000.v1



limit and the APS at it's lower size limit. This is supported also by the EM size distribution, which does not match in this region.

to the transition region of the upper size limit of the SMPS and the lower size limit of the APS.

Comparing the exhaust air data to the filtered exhaust air, the shape of the PSD is conserved, but the PN is reduced for over an order of magnitude. The remaining PN concentration in the ventilated air was at about ambient levels.

Interestingly, the comparison of the APS data at different measurement positions, shown in Figure 3(b), shows almost the same data for the measurement inside the test bed and the exhaust air measurement position, before the filter. This indicates that the emerging aerosol in the measurement chamber is transported relatively efficient through the ventilation system. But it is not known how this aerosol particles compare to RDE-NEP, neither how representative it is for NEP particles in general.

The obtained PN concentration data matches the observations from literature [6,31,32], that particles are observed in relevant quantities after the BDT exceeds a threshold temperature. We furthermore observed, that the level of particle emissions was repeatable and constant in terms of PSD and PN in our measurements from the third cycle on, after the BDT reached temperatures around 400 °C. This behaviour is illustrated in Figure 4(a) and was observed for every measured set. For a future possible follow-up measurement campaign a separation of SPN and TPN would be of interest.

Because of the given repeatability of the concentrations, the calculation and analysis of mean values is justified. We neglected the first two cycles of each set for the calculation of mean values. In Figure 4(b) the exemplary mean values of the PN concentration measured with the TSI 3775 and the BDT from one set are shown. The UFP PN concentration reaches over all considerable high values. A dependency to the BDT can be observed, which again is linked to the brake pressure. Stronger brake events, e.g. around second 40 or 70, cause a distinct increase in the BDT, which is then followed by an increase in the PN concentrations with a few seconds delay. Smaller brake events also cause a change in the BDT, but does not cause a clear increase in the PN concentration.

EM results from the samples drawn with the electrostatic sampler were against expectations. The PSD from all three deposition plates shows the same shape with decreasing numbers, as can be seen in Figure 5(a). 44.7 % of all particles were found at the 200 V plate, 38.6 % at the 400 V plate and 16.7 % at the 800 V plate. By inspection of the EM images of the three plates through the author, a qualitative difference between the deposited particles on the different plates appeared in their constitution. On the 200 V plate were rather compact particles, on the 400 V plate larger, mesh-like particles and on the 800 V plate were dominantly fractal particles.

Differences between the deposited particles on the different deposition plates can also be seen in the EDX analysis in Table 3. Oxygen is the only element which can be found in the majority of particles, independent of the sample. In the comparison of the particles from the three electrostatic sampling plates that iron was found in most particles at the 200 V plate and 400 V plate, but significantly less at the 800 V plate, although the mass fraction for iron is comparable. For magnesium the number, as well as the mass fraction are similar for the 200 V and the 400 V plate, but very different to the 800 V plate. For carbon the case is very peculiar in combination with the observation of fractal particles on the 800 V plate, as almost all found particles contain carbon. This is not the case for the other two plates, although the mass fraction is again comparable.

Separation of particles into BW and TW by tracer materials was not possible, as tracer materials for BW (e.g. iron, copper, lead and calcium [3]) have been found in the vast majority of particles. This could be interpreted in two ways, first the airborne particles in these measurements were dominantly BW particles, or second, the collected particles are secondary particles from all primary particle emitting sources in the test bed measurement chamber. Assuming the first thesis, it could also explain the peculiar match of the collected PM in the exhaust air filter to the mass loss of the brake pad and brake discs, listed in Table 1. However, based on current knowledge and the available data, this can neither be verified nor falsified.

 doi:10.20944/preprints202402.1000.v1



The here presented efforts must be contextualised as a feasibility study to measure particle emissions on a wheel and suspension test bed with a closed ventilation system. For future experiments it would be recommended to use a housing around wheel and brake, similar as defined for the measurement of brake emissions [33,34], with characterised losses and a well-defined flow profile. For better source appointment of the particle fractions, tyres, brake pads and discs with dedicated tracer materials should be used. Aerosol instrumentation for UFP should be used with dilution systems to operate in the ideal detection range. Furthermore, the sampling for EM analysis should be optimised in terms of flow design and the deposition voltages should cover a wider range.

## 5. Conclusions

Particle measurements have been done at a wheel and suspension test bed with a closed ventilation system for high-load driving scenarios, using an SMPS and an APS for PSD measurements, and a CPC for UFP concentration measurements. Samples have been collected for EM analysis with a custom made electrostatic sampler. The obtained results were consistent for all used measurement and analysis techniques. The exhaust air filter collected ∼25 % of the total mass loss of the wear components. The airborne fraction of the wear mass showed a high UFP mode at concentrations around 120 k#/cm$^3$ to 140 k#/cm$^3$ in the exhaust air flow. The PSD with the SMPS and the APS showed one distinct peak in the UFP region around 20 nm and considerable PN concentrations until 10 µm. The PSD was found to be consistent in the measurement chamber, the exhaust air flow the filtered exhaust air flow. As the PSD obtained with EM single particle analysis also matches the distribution from the aerosol instruments, also the PSD found in the exhaust air filter is consistent. The EM analysis of the samples with the different deposition voltages surprisingly also showed the same PSD for all plates, but differences in the constitution of the particles have been observed, also the chemical composition from the EDX analysis showed differences.

For further investigations of wear particles from a wheel and suspension test bed it is recommended to use a housing with a defined air flow and dilution factor around wheel and brake for ideally controlled measurement parameters. The sampling position inside the measurement chamber should be varied and, if necessary, optimised. For the PN measurements a separation of SPN and TPN would be of interest. Further investigations with electrostatic samplers and EM analysis should cover a wider range of deposition voltages.

**Author Contributions:** For research articles with several authors, a short paragraph specifying their individual contributions must be provided. The following statements should be used “Conceptualization, P.F., M.K. and H.S.; methodology, M.K., M.N, H.S. and P.F.; validation, M.K., H.S. and A.B.; formal analysis, M.K. and M.N.; investigation, L.S. and M.N.; resources, A.B. and P.F.; data curation, L.S., M.N. and M.K.; writing—original draft preparation, M.K.; writing—review and editing, M.K., L.S., M.N., H.S., M.H., A.B. and P.F.; visualization, M.K.; supervision, M.K., A.B. and P.F.; All authors have read and agreed to the published version of the manuscript.

**Funding:** This research received no external funding.

**Data Availability Statement:** The data presented in this study are available on request from the corresponding author.

**Acknowledgments:** The authors thank the organising team of the TAP conference in Gothenburg 2023 for the possibility to submit manuscripts of accepted conference contributions to the special issue "Transport Emissions and Their Environmental Impacts" of MDPI Atmosphere. Supported by TU Graz Open Access Publishing Fund.

**Conflicts of Interest:** The authors declare no conflict of interest.

 doi:10.20944/preprints202402.1000.v1



## Abbreviations

The following abbreviations are used in this manuscript:

| | |
|---|---|
| APS | Aerodynamic Particle Spectrometer |
| BDT | Brake Disc Temperature |
| BW | Brake Wear |
| CPC | Condenstation Particle Counter |
| DMA | Differential Mobility Analyser |
| ECD | Equivalent Circular Diameter |
| EDX | Energy-dispersive X-ray spectroscopy |
| EM | Electron Microscopy |
| GTR | Global Technical Regulation |
| OPS | Optical Particle Spectrometer |
| NEP | Non-Exhaust Particle |
| PM | Particulate Matter |
| PN | Particulate Number |
| PSD | Particle Size Distribution |
| RDE | Real Driving Emissions |
| SMPS | Scanning Mobility Particle Sizer |
| SPN | Solid Particulate Number |
| TPN | Total Particulate Number |
| TW | Tyre Wear |
| UFP | Ultra Fine Particles |

## Appendix A. Electrostatic Sampler

### *Appendix A.1. Description*

The sampler has a total length of 40 cm, consisting of a 10 cm inlet, 24 cm deposition area, containing four electrically separated deposition plates with a length of 5 cm, followed by a 6 cm outlet. The parts were manufactured by a 3D printer at the TU Graz. The flow channel in the deposition area has a height of 1 mm and width of 2.5 cm. The flow through the electrostatic sampler was constant at 1 L $min^{-1}$, provided by an membrane pump downstream.

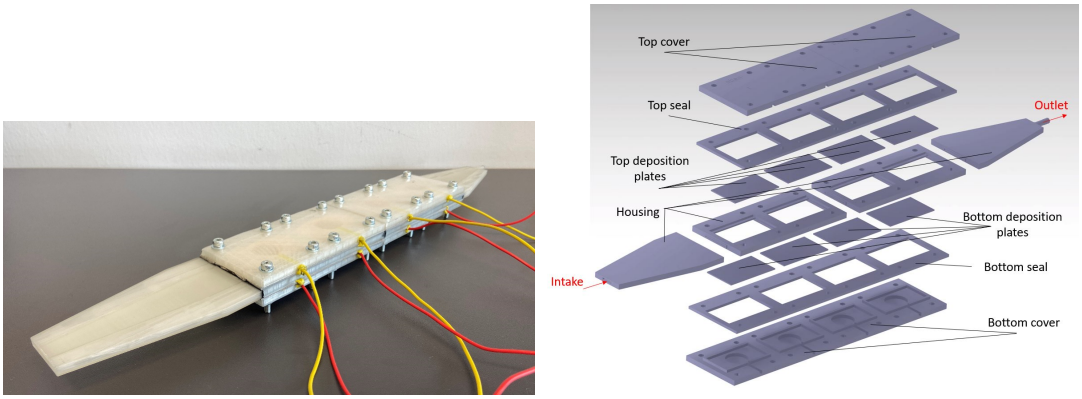


(a) Photography of the custom made electrostatic sampler (b) CAD of the electrostatic sampler.

**Figure A1.** The custom made electrostatic sampler

## Appendix B. Calculation

The calculation of the expected deposition sized was done according to [35] and the manual of the TSI 3080 electrostatic classifier, assuming one charge per particle.

 doi:10.20944/preprints202402.1000.v1



**Table A1.** Constants and parameters considered for the calculation. $\alpha$, $\beta$ and $\gamma$ are the factors used for the calculation of the Cunningham slip correction (CSP) factor.

| | Value | Unit |
|---|---|---|
| Mean free path | $6.730 \times 10^{-8}$ | m |
| Dynamic viscosity | $1.8325 \times 10^{-5}$ | $\mathrm{kg\,ms^{-1}}$ |
| Air pressure | 101.8 | kPa |
| Temperature | 310.15 | K |
| $\alpha$ (CSP) | 1.165 | - |
| $\beta$ (CSP) | 0.483 | - |
| $\gamma$ (CSP) | 0.997 | - |
| Volume flow | 1 | $\mathrm{L\,min^{-1}}$ |
| Permittivity air | 1.000 59 | $\mathrm{A\,s\,V^{-1}\,m^{-1}}$ |
| Entry | Data | Data |

## References


1. Sokhi, R.S.; Moussiopoulos, N.; Baklanov, A.; Bartzis, J.; Coll, I.; Finardi, S.; Friedrich, R.; Geels, C.; Grönholm, T.; Halenka, T.; et al. Advances in air quality research - current and emerging challenges. *Atmospheric Chemistry and Physics* **2022**, *22*, 4615–4703. https://doi.org/10.5194/acp-22-4615-2022.
2. European Environmental Agency, p. Air quality in Europe 2022, Web Reprt. https://www.eea.europa.eu/publications/air-quality-in-europe-2022, 2022. Accessed: 2023-12-22.
3. Harrison, R.M.; Allan, J.; Carruthers, D.; Heal, M.R.; Lewis, A.C.; Marner, B.; Murrells, T.; Williams, A. Non-exhaust vehicle emissions of particulate matter and VOC from road traffic: A review. *Atmospheric Environment* **2021**, *262*, 118592. https://doi.org/10.1016/j.atmosenv.2021.118592.
4. Piscitello, A.; Bianco, C.; Casasso, A.; Sethi, R. Non-exhaust traffic emissions: Sources, characterization, and mitigation measures. *Science of the Total Environment* **2021**, *766*, 144440. https://doi.org/10.1016/j.scitotenv.2020.144440.
5. Grigoratos, T.; Martini, G. Brake wear particle emissions: a review. *Environmental Science and Pollution Research* **2015**, *22*, 2491–2504. https://doi.org/10.1007/s11356-014-3696-8.
6. Stojanovic, N.; Glisovic, J.; Abdullah, O.I.; Belhocine, A.; Grujic, I. Particle formation due to brake wear, influence on the people health and measures for their reduction: a review. *Environmental Science and Pollution Research* **2022**, *29*, 9606–9625. https://doi.org/10.1007/s11356-021-17907-3.
7. Giechaskiel, B.; Grigoratos, T.; Mathissen, M.; Quik, J.; Tromp, P.; Gustafsson, M.; Franco, V.; Dilara, P. Contribution of Road Vehicle Tyre Wear to Microplastics and Ambient Air Pollution. *Sustainability* **2024**, *16*, 522. https://doi.org/10.3390/su16020522.
8. Bondorf, L.; Köhler, L.; Grein, T.; Epple, F.; Philipps, F.; Aigner, M.; Schripp, T. Airborne Brake Wear Emissions from a Battery Electric Vehicle. *Atmosphere* **2023**, *14*. https://doi.org/10.3390/atmos14030488.
9. Dimopoulos Eggenschwiler, P.; Schreiber, D.; Habersatter, J. Brake Particle PN and PM Emissions of a Hybrid Light Duty Vehicle Measured on the Chassis Dynamometer. *Atmosphere* **2023**, *14*. https://doi.org/10.3390/atmos14050784.
10. Giechaskiel, B.; Grigoratos, T.; Dilara, P.; Karageorgiou, T.; Ntziachristos, L.; Samaras, Z. Light-Duty Vehicle Brake Emission Factors. *Atmosphere* **2024**, *15*, 1–20. https://doi.org/10.3390/atmos15010097.
11. Council of the European Union, p. Press Release - Euro 7: Council and Parliament strike provisional deal on emissions limits for road vehicles. https://www.consilium.europa.eu/en/press/press-releases/2023/12/18/euro-7-council-and-parliament-strike-provisional-deal-on-emissions-limits-for-road-vehicles/#:~:text=With%20Euro%207%20we%20aim,zero%20emissions%20vehicles%20by%202035., 2023. Accessed: 2023-12-22.
12. Grigoratos, T.; Mathissen, M.; Vedula, R.T.; Mamakos, A.; Agudelo, C.; Gramstat, S.; Giechaskiel, B. Interlaboratory Study on Brake Particle Emissions—Part I: Particulate Matter Mass Emissions. *Atmosphere* **2023**, *14*. https://doi.org/10.3390/atmos14030498.
13. Mathissen, M.; Grigoratos, T.; Gramstat, S.; Mamakos, A.; Vedula, R.T.; Agudelo, C.; Grochowicz, J.; Giechaskiel, B. Interlaboratory Study on Brake Particle Emissions Part II: Particle Number Emissions. *Atmosphere* **2023**, *14*. https://doi.org/10.3390/atmos14030424.

14. Grigoratos, T.; Mamakos, A.; Arndt, M.; Lugovyy, D.; Anderson, R.; Hafenmayer, C.; Moisio, M.; Vanhanen, J.; Frazee, R.; Agudelo, C.; et al. Characterization of Particle Number Setups for Measuring Brake Particle Emissions and Comparison with Exhaust Setups. *Atmosphere* **2023**, *14*, 103. https://doi.org/10.3390/atmos14010103.
15. Giechaskiel, B.; Melas, A.; Martini, G.; Dilara, P.; Ntziachristos, L. Revisiting Total Particle Number Measurements for Vehicle Exhaust Regulations. *Atmosphere* **2022**, *13*, 1–36. https://doi.org/10.3390/atmos13020155.
16. Mamakos, A.; Arndt, M.; Hesse, D.; Augsburg, K. Physical characterization of brake-wear particles in a PM10 dilution tunnel. *Atmosphere* **2019**, *10*. https://doi.org/10.3390/atmos10110639.
17. Farwick zum Hagen, F.H.; Mathissen, M.; Grabiec, T.; Hennicke, T.; Rettig, M.; Grochowicz, J.; Vogt, R.; Benter, T. On-road vehicle measurements of brake wear particle emissions. *Atmospheric Environment* **2019**, *217*, 116943. https://doi.org/10.1016/j.atmosenv.2019.116943.
18. Huber, M.P.; Fischer, P.; Murg, J.; Reingruber, H.; Wanek-Ruediger, C.; Weidinger, C.; Steiner, G. Characterizing a Real-Driving Brake Emissions Sampling System on a Laboratory Test Bed. *SAE Technical Papers* **2023**, pp. 1–13. https://doi.org/10.4271/2023-01-1875.
19. Huber, M.P.; Fischer, P.; Mamakos, A.; Steiner, G.; Klug, A. Measuring Brake Wear Particles with a Real-Driving Emissions Sampling System on a Brake Dynamometer. *SAE Technical Papers* **2022**, pp. 1–15. https://doi.org/10.4271/2022-01-1180.
20. Fussell, J.C.; Franklin, M.; Green, D.C.; Gustafsson, M.; Harrison, R.M.; Hicks, W.; Kelly, F.J.; Kishta, F.; Miller, M.R.; Mudway, I.S.; et al. A Review of Road Traffic-Derived Non-Exhaust Particles: Emissions, Physicochemical Characteristics, Health Risks, and Mitigation Measures. *Environmental Science and Technology* **2022**, *56*, 6813–6835. https://doi.org/10.1021/acs.est.2c01072.
21. Hesse, D.; Feißel, T.; Kunze, M.; Bachmann, E.; Bachmann, T.; Gramstat, S. Comparison of Methods for Sampling Particulate Emissions from Tires under Different Test Environments. *Atmosphere* **2022**, *13*. https://doi.org/10.3390/atmos13081262.
22. Schläfle, S.; Unrau, H.J.; Gauterin, F. Influence of Load Condition, Tire Type, and Ambient Temperature on the Emission of Tire–Road Particulate Matter. *Atmosphere* **2023**, *14*. https://doi.org/10.3390/atmos14071095.
23. Grigoratos, T.; Gustafsson, M.; Eriksson, O.; Martini, G. Experimental investigation of tread wear and particle emission from tyres with different treadwear marking. *Atmospheric Environment* **2018**, *182*, 200–212. https://doi.org/10.1016/j.atmosenv.2018.03.049.
24. Giechaskiel, B.; Dilara, P.; Sandbach, E.; Andersson, J. Particle measurement programme (PMP) light-duty inter-laboratory exercise: comparison of different particle number measurement systems. *Measurement Science and Technology* **2008**, *19*, 095401. https://doi.org/10.1088/0957-0233/19/9/095401.
25. Schurl, S.; Kupper, M.; Krasa, H.; Schmidt, S.; Sturm, S.; Heidinger, A. A PN-Measurement System for Small Engine Applications. *SAE Technical Papers* **2023**, pp. 1–7. https://doi.org/10.4271/2023-01-1809.
26. Giechaskiel, B.; Wang, X.; Gilliland, D.; Drossinos, Y. The effect of particle chemical composition on the activation probability in n-butanol condensation particle counters. *Journal of Aerosol Science* **2011**, *42*, 20–37. https://doi.org/10.1016/j.jaerosci.2010.10.006.
27. Wlasits, P.J.; Stolzenburg, D.; Tauber, C.; Brilke, S.; Schmitt, S.H.; Winkler, P.M.; Wimmer, D. Counting on chemistry: Laboratory evaluation of seed-material-dependent detection efficiencies of ultrafine condensation particle counters. *Atmospheric Measurement Techniques* **2020**, *13*, 3787–3798. https://doi.org/10.5194/amt-13-3787-2020.
28. Krasa, H.; Kupper, M.; Schriefl, M.A.; Bergmann, A. Toward a simplified calibration method for 23 nm automotive particle counters using atomized inorganic salt particles. *Aerosol Science and Technology* **2023**, *57*, 329–341. https://doi.org/10.1080/02786826.2023.2174410.
29. Gasser, E. Characterization of Gas and Particle Released during Thermal Runaway of Li-Ion Batteries. *Master's Thesis, Graz University of Technology, Graz, Austria* **2019**, pp. 2–92.
30. Mathissen, M.; Grochowicz, J.; Schmidt, C.; Vogt, R.; Farwick zum Hagen, F.H.; Grabiec, T.; Steven, H.; Grigoratos, T. A novel real-world braking cycle for studying brake wear particle emissions. *Wear* **2018**, *414-415*, 219–226. https://doi.org/10.1016/j.wear.2018.07.020.
31. Wang, Y.; Yin, H.; Yang, Z.; Su, S.; Hao, L.; Tan, J.; Wang, X.; Niu, Z.; Ge, Y. Assessing the brake particle emissions for sustainable transport: A review. *Renewable and Sustainable Energy Reviews* **2022**, *167*, 112737. https://doi.org/10.1016/j.rser.2022.112737.

32. Asbach, C.; Todea, A.M.; Zessinger, M.; Kaminski, H. Entstehung und Möglichkeiten zur Messung von Fein- und Ultrafeinstaub beim Bremsen; 2019; pp. 45–67. https://doi.org/10.1007/978-3-662-58024-0_4.
33. Mamakos, A.; Huber, M.P.; Arndt, M.; Reingruber, H.; Steiner, G.; Weidinger, C. Design of a Laboratory Sampling System for Brake Wear Particle Measurements. *SAE Technical Papers* **2022**, *1*, 1–11. https://doi.org/10.4271/2022-01-1179.
34. Mathissen, M.; Grigoratos, T.; Gramstat, S.; Mamakos, A.; Vedula, R.T.; Agudelo, C.; Grochowicz, J.; Giechaskiel, B. Interlaboratory Study on Brake Particle Emissions Part II: Particle Number Emissions. *Atmosphere* **2023**, *14*. https://doi.org/10.3390/atmos14030424.
35. Bilby, D.; Kubinski, D.J.; Maricq, M.M. Current amplification in an electrostatic trap by soot dendrite growth and fragmentation: Application to soot sensors. *Journal of Aerosol Science* **2015**, *98*, 41–58. https://doi.org/10.1016/j.jaerosci.2016.03.003.